



Published in final edited form as:

Nanomedicine. 2016 January ; 12(1): 109–122. doi:10.1016/j.nano.2015.09.009.

The Mixed Lineage Kinase-3 Inhibitor URMC-099 Improves Therapeutic Outcomes for Long-Acting Antiretroviral Therapy

Gang Zhang^{1,+}, Dongwei Guo^{1,2,+}, Prasanta K. Dash^{1,+}, Mariluz Araínga¹, Jayme L. Wiederin^{1,3}, Nicole A Haverland^{1,†}, Jaclyn Knibbe-Hollinger¹, Andrea Martinez-Skinner¹, Pawel Ciborowski¹, Val S. Goodfellow⁴, Tadeusz A. Wysocki⁵, Beata J. Wysocki⁵, Larisa Y. Poluektova¹, Xin-Ming Liu^{1,2,§}, JoEllyn M. McMillan¹, Santhi Gorantla¹, Harris A. Gelbard⁶, and Howard E. Gendelman^{1,2,*}

¹Department of Pharmacology and Experimental Neuroscience University of Nebraska Medical Center, Omaha, NE, 68198-5880 USA

²Department of Pharmaceutical Sciences, University of Nebraska Medical Center, Omaha, NE, 68198-5880 USA

³Office of the Vice Chancellor for Research, University of Nebraska Medical Center, Omaha, NE, 68198-7878 USA

⁴Califia Bio, San Diego, CA, 92121 USA

⁵Department of Computer and Electronics Engineering, University of Nebraska-Lincoln, Omaha, NE, 68182-0572 USA

⁶Department of Neurology, Center for Neural Development & Disease, School of Medicine and Dentistry, University of Rochester Medical Center, Rochester, NY, 14642 USA

Abstract

During studies to extend the half-life of crystalline nanoformulated antiretroviral therapy (nanoART) the mixed lineage kinase-3 inhibitor URMC-099, developed as an adjunctive neuroprotective agent was shown to facilitate antiviral responses. Long-acting ritonavir-boosted

¹**Abbreviations:** nanoART, nanoformulated antiretroviral therapy; nanoATV/r, long acting nanoformulated ritonavir boosted atazanavir; NSG mice, NOD/SCID/IL2R γ c^{-/-} mice; MP, mononuclear phagocytes; CYP3A, cytochrome P450 3A; VL, viral load; MDM, monocyte-derived macrophages; IRB, Institutional Review Board; FA-nanoART, folic acid-modified nanoART; RT, HIV-1 reverse transcriptase; ATV, atazanavir; r/RTV, ritonavir; P407, poloxamer 407; TCID₅₀, tissue culture infective dose 50; DAVID, Database for Annotation, Visualization and Integrated Discovery; KEGG, Kyoto Encyclopedia of Genes and Genomes; PFA, paraformaldehyde; MLK3, mixed lineage kinase 3; SWATH-MS, Sequential Windowed data independent Acquisition of the Total High-resolution Mass Spectra; MOI, multiplicity of infection.

Address correspondence to: Dr. Howard E. Gendelman, Department of Pharmacology and Experimental Neuroscience, 985880 Nebraska Medical Center, Omaha, NE, USA 68198-5880, Phone: (402) 559-8920, Fax: (402) 559-3744, hegendel@unmc.edu.

[†]Current Address: Department of Chemistry, Northwestern University, Evanston, IL, 60208, USA

[§]Current Address: United States Food and Drug Administration, Silver Spring, MD, 20993-0002, USA

⁺Equal contributions

Competing interests: H.A.G. and H.E.G. are members of the Scientific Advisory Board of WavoDyne Therapeutics, Inc. that has exclusive rights to URMC-099 development.

Publisher's Disclaimer: This is a PDF file of an unedited manuscript that has been accepted for publication. As a service to our customers we are providing this early version of the manuscript. The manuscript will undergo copyediting, typesetting, and review of the resulting proof before it is published in its final citable form. Please note that during the production process errors may be discovered which could affect the content, and all legal disclaimers that apply to the journal pertain.

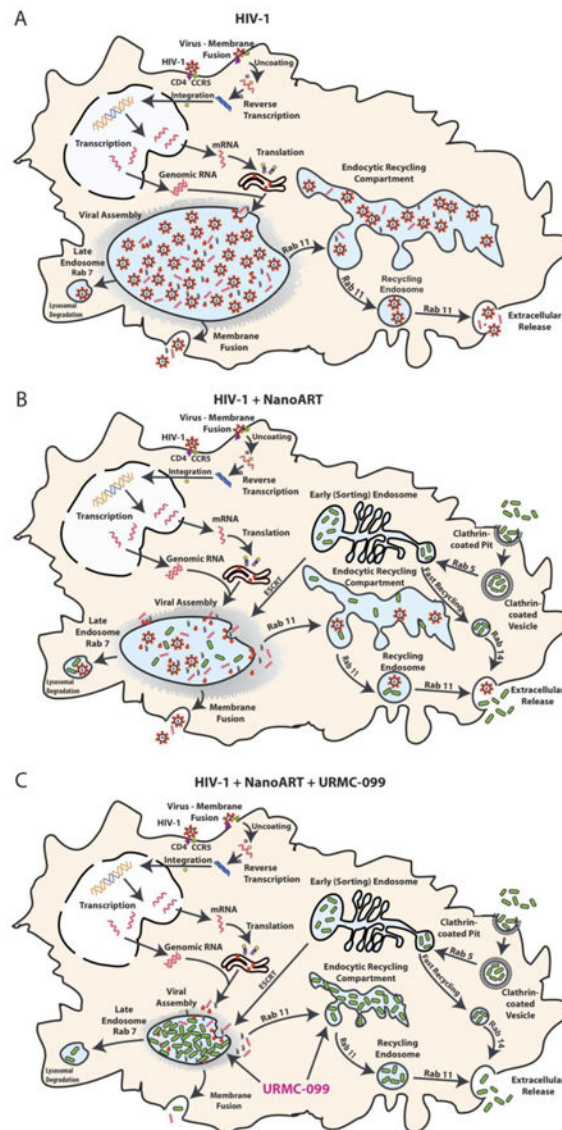
atazanavir (nanoATV/r) nanoformulations co-administered with URM-099 reduced viral load and the numbers of HIV-1 infected CD4+ T-cells in lymphoid tissues more than either drug alone in infected humanized NOD/SCID/IL2R γ ^{-/-} mice. The drug effects were associated with sustained ART depots. Proteomics analyses demonstrated that the antiretroviral responses were linked to affected phagolysosomal storage pathways leading to sequestration of nanoATV/r in Rab-associated recycling and late endosomes; sites associated with viral maturation. URM-099 administered with nanoATV induced a dose-dependent reduction in HIV-1p24 and reverse transcriptase activity. This drug combination offers a unique chemical marriage for cell-based viral clearance.

Graphical Abstract: Figure 8.¹

Abstract

Graphical abstract text

Schematic diagrams reveal URM-099 affects nanoART endosomal trafficking and HIV-1 progeny virion production. (A) HIV-1 budding, assembly and maturation in macrophage Rab7 and Rab11 endosomal compartments. (B) NanoATV targets endosomal compartment for storage and inhibits viral maturation at the site of viral assembly. (C) URM-099 boosts nanoATV antiviral activity through increased nanoATV accumulation in macrophage Rab7 and Rab11 endosomal compartments.



Keywords

HIV-1; Long-acting nanoformulations; URMC-099; Humanized mice; Phagolysosome; Rab proteins

Introduction

Long-acting nanoformulated antiretroviral therapy (nanoART) offers advantages for the management of human immunodeficiency virus type one (HIV-1) infection¹. Long-lived intracellular drug depots, at or adjacent to the viral life cycle, can improve both regimen adherence and antiretroviral responses². NanoART could affect chemical viral eradication^{3,4}. The accumulation of nanoART particles in late and recycling mononuclear phagocyte (MP: monocytes, macrophages and dendritic cells) endosomes^{1,5-7} can limit

hepatic ART metabolism and renal secretion⁸⁻¹⁰. Metabolism of HIV-1 protease inhibitors by hepatic cytochrome P450 3A (CYP3A)^{11, 12} may also be slowed by drug intracellular carriage. However, the limitations of nanoART reside in the effectiveness of the cells' depot storage capacity. We posit that the longer the storage the longer the drug half-life. As preventative vaccines for HIV have thus far proven ineffective, extending the time intervals for ART administration could serve as effective pre-exposure prophylaxis measures and as surrogate vaccination measures. Moreover, drug patient adherence to complex regimens may also be improved as the effectiveness of ART has been plagued by limitations in taking the drugs at needed time intervals. Novel platforms designed to achieve such goals represent “cutting edge” bench to bedside research pursuits.

To such ends we now report a novel means to perpetuate the ART depot in subcellular organelles. The discovery was made during the evaluation of the mixed lineage kinase-3 (MLK3) inhibitor URM-099 as an adjunctive neuroprotective HIV/AIDS therapy^{13, 14}. Here we have shown potentiation of nanoART effected antiretroviral responses. HIV-1 infected, nanoART- and URM-099-treated humanized NOD/SCID/IL2R γ ^{-/-} (NSG) mice showed reductions in viral load (VL) and decreased numbers of infected lymphocytes in spleen and lymph nodes with restoration of CD4⁺ T-cells in peripheral blood. In HIV-1 infected human monocyte-derived macrophages (MDM), URM-099 increased nanoART retention in recycling and late Rab protein-associated endosomes. URM-099 facilitated nanoART actions by reducing residual HIV-1 in infected NSG mice. Reduction of virus to undetectable levels beyond what either drug can achieve alone was observed. Notably, virus-infected lymphocytes were not observed in such treated and infected animals. The establishment of an extended ART depot in monocyte-macrophages is a significant step forward in development of long-acting ART strategies for HIV/AIDS. Moreover, combination of URM-099 and nanoART can extend ART half-life and improve treatment outcomes for those infected while also serving to protect those at risk for infection.

Methods

Ethics Statement

All animal studies were approved by the Institutional Animal Care and Use Committee of the University of Nebraska Medical Center (UNMC). Animal studies were performed in compliance with UNMC institutional policies and the National Institutes of Health (NIH) guidelines for housing and care of laboratory animals. Human tissues were obtained from University of Washington, supported by NIH award 5R24HD000836. These studies were approved by the UNMC Institutional Review Board (IRB), in accordance with Health and Human Services Regulations, for the protection of human subjects. All fetal liver tissues were anonymized without patient information or identifiers when obtained. Human monocytes were isolated by leukopheresis from HIV-1/2 and hepatitis seronegative donors according to an approved UNMC IRB exempt protocol.

Study design

The MLK3 inhibitor URM-099 was tested for its abilities to affect nanoART antiretroviral activities. *First*, URM-099 was administered to an HIV-1-infected humanized mouse

model treated with folic acid decorated-nanoART (FA-nanoART) and antiretroviral drug concentrations measured in plasma and tissues. *Second*, putative mechanisms of URM-099 action against HIV-1 infection were examined by SWATH proteomics and Western blot. *Third*, HIV-1 integrated viral DNA, RNA, HIV-1p24 protein and HIV-reverse transcriptase (RT) activities were measured. *Fourth*, URM-099-induced nanoART retention in cells and cellular compartments was determined by endosomal immunoaffinity isolation, HPLC drug analysis, mathematical simulation and confocal microscopy.

Preparation of nanoformulated ATV/r

Folic acid-conjugated-P407 was synthesized as previously described^{15, 16}. Folate-targeted and non-targeted nanoformulations of atazanavir (ATV) and ritonavir (r. RTV) were prepared as described in the Supplement. Fluorescently-labeled nanoART was made and purified with CF568-modified P407 or CF633-modified P188.¹⁵

Viral infection and treatment of CD34+ NSG mice

NSG mice were reconstituted with human fetal hematopoietic CD34+ stem cells as previously described⁶. After 22-26 weeks, mice were infected intraperitoneally (IP) with HIV-1_{ADA} at 10⁴ TCID₅₀/mouse. Ten weeks after infection, mice were given URM-099 (10 mg/kg, IP) daily for three weeks with weekly intramuscular (IM) injections of 100 mg/kg folate-modified nanoATV/r (FA-nanoATV/r) (1:1). One week after the third FA-nanoATV/r injection spleen, brain, liver and plasma were collected for drug levels and antiviral activity determination¹⁷

Immunohistochemistry

Immunohistochemistry on spleen and lymph nodes were performed⁶. Tissues were stained for HLA-DR, CD45 and HIV-1p24. Spleen sections were double stained with antibodies to human CD3, CD68, Rab7 and HIV-1p24. Immunofluorescence staining was captured using a LSM 510 confocal microscope (Carl Zeiss Microimaging Inc., Dublin, CA) or by Nuance microscopy⁶. Replicate tissues were collected from BALB/c mice 12 hours-post IP injection with 100 mg/kg CF633-labeled nanoATV and flash-frozen in Tissue-Tek O.C.T. Cryosections were stained with antibodies to F4/80 (Abeam, Cambridge, MA) followed by a Alexa Fluor 488 conjugated secondary antibody.

Monocyte-macrophage cultures

Human MDM cultures were established as previously described¹⁸.

SWATH-MS proteomics and data analyses

Human MDM were infected with HIV-1_{ADA} for 4 hours, treated with/without 100 μM nanoATV and 10 ng/mL URM-099 for 16 hours. Cells were harvested and proteins digested¹⁹. Database for Annotation, Visualization and Integrated Discovery (DAVID) bioinformatic resource 6.7 was used for high-stringency functional annotation clustering for protein identification²⁰. The Kyoto Encyclopedia of Genes and Genomes (KEGG) Mapper Search & Color Pathway tool was used to visualize the endocytosis pathway with proteomics data overlay^{21, 22}.

NanoATV and URM-099 treatment

MDM were treated with 100 μ M native ATV or nanoATV with or without 0.1 to 100 ng/ml of URM-099. After 16 hours, MDM were infected with HIV-1_{ADA} at an MOI of 0.1 for 4 hours on day 0, 5 or 10 after drug loading. Cells were cultured for an additional 2 weeks in the absence or presence of URM-099.

Western blots

Western blots on MDM were performed as described²³ and membranes were probed with Rab5, -7, -11, LAMP1 or STAT1 antibodies.

HIV-1 measurements

MDM were treated with nanoATV and URM-099, infected on day-0 with HIV-1_{ADA} and cultured for an additional 14-days. Genomic DNA from MDM was extracted using the Puregene Core Kit. Integrated HIV-1 DNA was assessed by Alu-gag real time PCR using a modified protocol²⁴. The HIV standards were generated DNA H3B, ACH-2 and 8E5 cell lines²⁵. In replicate wells, RNA from MDM was isolated using RNeasy mini kit (Qiagen). HIV-1 gag RNA was assessed by real-time RT-PCR²⁶. Culture media were collected until 14-days from HIV-1-infected MDM for RT activity measures as previously described⁹. HIV-1p24 staining was performed as described.

MDM nanoATV uptake and retention and endocytic trafficking

Uptake and retention of nanoATV in MDM were studied²⁷. MDM cultured on LabTek CC₂ chamber slides were treated with 100 μ M CF-568-labeled nanoATV with or without 10 ng/mL URM-099 for 16 hours. Following HIV-1_{ADA} infection at a MOI of 0.1 for 4 hours, the infected MDM were cultured for an additional 14 days with 0 or 10 ng/ml URM-099. MDM not infected with HIV-1_{ADA} were cultured for 12, 24, 48 or 144 hours after nanoART loading with 0 or 10 ng/ml URM-099. All cells (infected and non-infected) were fixed with ice-cold 4% PFA for 30 min, treated with permeabilizing/blocking solution (0.1% Triton, 5% BSA in PBS) then incubated with rabbit anti-human Rab7 or 11 or mouse anti-human HIV-1p24. Alexa Fluor 488 goat anti-rabbit secondary antibody detected Rab7 and 11 antibodies and Alexa Fluor 633 goat anti-mouse secondary antibody was used for HIV-1p24. Slides were covered with ProLong Gold anti-fade reagent with DAPI and imaged on a LSM 510 confocal microscope (Carl Zeiss Microimaging Inc.). Double or triple co-localization images were analyzed using Zeiss LSM 510 Image browser AIM software version 4.2 and Image J (NIH, Bethesda, MD) software with BlobProb plug-in for percent overlap⁸.

Statistical analyses

The sample size was determined according to published guidelines with a minimum of 5 animals per group (n = 5). All experiments were replicated three times and results were blinded until statistical analyses. No outliers from animal or cell experiments were excluded. Data comparisons were analyzed using Prism (GraphPad Software Inc, La Jolla, CA). One-way ANOVA was used to compare three or more samples followed by unpaired, two-tailed

Student's *t*-test. Student's *t*-test was also used to compare two samples. All significant differences were determined at $p < 0.05$.

Results

URMC-099 potentiates nanoART activities in humanized CD34+ NSG mice

Chronic immune activation potentiates HIV-1 infection and CD4⁺ T-cell loss²⁸⁻³⁰. Notably, immune deactivation reduces pro-inflammatory activities and end-organ tissue injury³¹⁻³³. Recently, URMC-099, a MLK3 inhibitor with excellent end-organ pharmacokinetic profiles became available to our laboratory based on its effectiveness as an anti-inflammatory neuroprotective agent^{14, 34}. We reasoned that it could potentiate nanoART as inflammation regulates Rab endosomal networks and extend drug depot sites⁸. Thus, we reasoned that URMC-099 would extend drug nanoparticle activities^{35, 36}. To test this idea human CD34⁺ hematopoietic-reconstituted NSG mice were infected with HIV-1_{ADA} at a tissue culture infective dose of 0.1 infectious virions/ml for nine weeks. Infected mice were divided into untreated controls, URMC-099 treated, FA-nanoATV/r treated or both. To facilitate particle entry into cells, FA was used as the targeting ligand for nanoATV/r.^{15, 16} FA-nanoATV/r was administered once a week with daily URMC-099 for three weeks. FACS tests of peripheral blood over 13-weeks demonstrated significant gradual depletion of CD4⁺ T-cells in HIV-1 infected mice when compared to uninfected controls (Figure 1A). In HIV-1 infected mice, CD4⁺ T-lymphocytes were restored in the FA-nanoATV/r and URMC-099 co-administered group when compared to URMC-099 only treated mice (Figure 1B). Before starting treatment regimens, the median plasma VL in infected mice was 10⁵ copies/ml. Mice treated with FA-nanoATV/r had a mean plasma VL of 1.6×10^3 copies/ml. Mice treated with URMC-099 and FA-nanoATV/r had mean VL of 284 copies/ml, a 5.6-fold reduction over FA-nanoATV/r treatment alone ($p < 0.01$, Figure 1C). Treatment with URMC-099 alone did not affect the VL compared to infected controls (NS, $p = 0.2$). Immunohistochemical staining for HIV-1p24 in spleen confirmed the VL tests (Figure 2A). Untreated, infected animals had 40 HIV-1p24⁺ cells/1000 CD45⁺ cells in spleen. After three weeks of FA-nanoATV/r treatment, HIV-1p24⁺ cells were reduced to 4 HIV-1p24⁺ cells/1000 CD45⁺ cells ($p < 0.01$; Figure 2A and C). Treatment with URMC-099 and FA-nanoATV/r further reduced this number to < 0.1 HIV-1p24/1000 CD45⁺ cells ($p < 0.001$; Figure 2A and C). Double immunofluorescence staining for human CD3 and HIV-1p24 showed that the decreases were in numbers of infected T-cells (Figure 2E). Pharmacokinetic analyses showed increases in RTV from 411 to 1053 ng/g and 1471 to 3238 ng/g in spleen and liver ($p < 0.05$) co-administered with URMC-099 (Supplemental Figure 1A and B). ATV levels were also increased from 215 to 326 ng/g in spleen, but the differences did not reach statistical significance ($p = 0.065$) (Supplemental Figure 1C). No differences in liver ATV levels were seen (Supplemental Figure 1D).

URMC-099 facilitates nanoATV/r antiretroviral activities in lymph nodes

Elimination of HIV-1p24⁺ cells in lymph nodes, by non-targeted nanoATV/r, was not achieved in humanized NSG mice⁶. In this study, HIV-1p24⁺ HLA-DR⁺ cells in lymph nodes were reduced in URMC-099 and FA-nanoATV/r treated mice. Untreated, infected animals had 50.3 HIV-1p24 cells/1000 CD45⁺ cells in lymph nodes. Three weeks of FA-

nanoATV/r treatment significantly reduced the number of HIV-1p24+ cells to 10.8 HIV-1p24 cells/1000 HLA-DR+ cells ($p < 0.005$; Figure 2B and D). but treatment with URM-099 and FA-nanoATV/r further reduced this number to < 2.3 HIV-1p24/1000 HLA-DR+ cells ($p < 0.001$; Figure 2B and D).

Proteomic analyses of virus-infected MDM

We theorized that the locus of URM-099's interactions with nanoATV could be the site of virion assembly based on ATV's action. Thus, we focused our investigation on the effects of HIV-1 infection on the host cell proteome³⁷⁻⁴¹, particularly in cellular organelles where the virus is assembled in macrophages^{10, 42}. As nanoATV/r accumulates in macrophages the gradual elimination of the viral T cell reservoir is linked to drug release from its intracellular depots. To assess the effects of nanoATV/r and URM-099 treatments on viral replication in macrophages, proteomic tests of whole cell lysates were performed using Sequential Windowed data independent Acquisition of the Total High-resolution Mass Spectra (SWATH-MS) (36-38). Quantitative profiling of HIV-1 infected human MDM demonstrated 181 up-regulated and 162 down-regulated protein species ($p < 0.05$) in four replicate samples evaluated by the paired-samples Z-test as compared to uninfected cells (Supplemental Figure 3A-B). DAVID and KEGG bio informatics tools enabled functional enrichment and pathway analyses on a dataset of 438 proteins. The effect of HIV-1 infection, URM-099 and nanoATV is summarized in Table 1 and Figure 3A-B). Few numbers of proteins were altered as a consequence of URM-099 or nanoATV treatment in uninfected MDM. Rab5 and -7, specifically, were upregulated by viral infection. This result was in agreement with our prior findings^{8,43-45}. Proteins deregulated by URM-099 and nanoATV included Rab5, TfR, vATPase and FcγR. Opposing regulation of phagolysosomal and endosomal proteins between HIV-1 infection and those virus-infected treated with nanoATV with and without URM-099 were found. To determine if URM-099 could alter the expression of Rab proteins beyond what was seen by nanoATV, we examined the effects of URM-099 and nanoATV in HIV-1-infected or uninfected MDM. Quantitative Western blot analyses of cell lysates showed increases in Rab5, -7 and LAMP1 expressions in infected macrophages treated with increasing concentrations of URM-099 alone compared with uninfected macrophages (Figure 3C-D). Importantly, co-treatment of uninfected and virus-infected MDM with nanoATV and URM-099 led to reductions in Rab5, -7, STAT1 and LAMP1 expressions. These reductions were more significant in HIV-1 infected cells for Rab7, STAT1 and LAMP1. In the combined treatment groups, with the increasing URM-099 concentrations, the greatest decreases were in Rab7, STAT1 and LAMP1.

Localization and regulation of Rab proteins in macrophages containing nanoATV/r

To confirm these proteomics results for nanoART-macrophage interactions, we determined the cellular distribution and subcellular localization of nanoATV/r *in vivo* by injecting CF633 dye labeled nanoATV/r into mice. Splenic and hepatic tissues were recovered after animal sacrifice then stained with F4/80 antibodies to identify macrophages. CF633 dye co-localized in macrophages (Figure 4A) but not CD3 positive T cells in the reticuloendothelial system. In HIV-1 infected humanized NSG mice, Rab7 expression was increased when compared to uninfected controls ($p = 0.0003$; Figure 4B and C). A decrease of Rab7 expression, by 50%, was observed within human macrophages in infected NSG mice treated

with URM-099 or with nanoATV/r and URM-099 compared to mice treated with nanoART/r alone ($p < 0.01$ and 0.001 , respectively, Figure 4B). Immunofluorescence quantitation showed that Rab7 levels were similar in murine macrophages likely as a result of macrophage viral infection in human cells (Supplemental Figure 2A-B).

URM-099 potentiates nanoATV antiretroviral activities

Human MDM endosomes harbor both progeny virus and ART nanoparticles⁸. To assess how these drugs could influence viral replication we treated MDM with nanoATV and or URM-099 prior to viral exposure. After 14-days of HIV-1_{ADA} infection administered at a multiplicity of infection (MOI) of 0.1, integrated HIV-1 DNA was measured by Alu-long terminal repeat (LTR)-based real-time nested PCR. URM-099 had no effect on HIV-1 DNA in infected MDM. Administration of nanoATV reduced HIV-1 integrated DNA (74 copies per 1000 cells with nanoATV compared to 11,471 copies/1000 cells without nanoATV). Further, suppression to 33 copies per 1000 cells was observed when URM-099 and nanoATV were co-administered (Figure 5A). Reductions in RNA levels to 19 copies of HIV-1p24 gag RNA per MDM were seen, 3-fold less than with nanoATV alone ($p < 0.05$; Figure 5B). URM-099 also significantly boosted antiretroviral effects of native ATV, although to a markedly lesser extent. HIV-1p24 viral RNA was reduced to 1885 copies/cell following native ATV treatment and reduced in a dose-dependent manner to 1250, 725 and 663 copies after co-treatment with 0.1, 1 and 10 ng/ml URM-099. Treatment with URM-099 alone did not affect HIV-1 integrated DNA and viral RNA levels. Immunofluorescence staining of HIV-1p24 antigen in MDM showed parallel reductions after URM-099 and nanoATV treatments (Figure 5C). NanoATV treatment alone resulted in a decrease in HIV-1p24 expression of 90.8%, 94.2% and 95.7% with 1, 10 and 100 μM nanoATV respectively. Co-treatment with URM-099 (0.1, 1, 10 and 100 ng/ml) enhanced nanoATV HIV-1p24 suppression by 63.8, 81.7, 87.8 and 91.3%, respectively ($p < 0.05$) (Figure 5C). These results signaled the abilities of nanoATV and URM-099 to work in tandem to reduce viral production but the pathway for such effects remain unclear.

To cross validate the HIV-1p24 assays and to substantiate the antiretroviral efficacy of nanoATV and URM-099 we next determined levels of HIV-1 reverse transcriptase (RT) activity in cell culture supernatants. Human MDM were treated with increasing concentrations of native or nanoATV (0.1, 1, 10 and 100 μM) with or without 0.1 or 1 ng/ml URM-099. The cells were then infected with HIV-1_{ADA} at an MOI of 0.1 for 4 hours at day 0, 5 or 10 (Figure 6A-B, Supplemental Figure 4). RT activity was measured over 14 days following viral infection. The rationale for waiting up to 10 days to infect the MDM rested in the idea that URM-099 would affect the ATV depot and as consequence extend the drug half-life. In cells infected on day-0, nanoATV at 0.1 μM suppressed RT activity by approximately 10-fold while concentrations of 1-100 μM suppressed RT activity to detectable limits of assay. Co-treatment with URM-099 (0.1 or 1 ng/ml) reduced RT activity at all nanoATV concentrations. When the time of HIV-1 infection was delayed to days-5 or 10 after drug treatments, co-administration of URM-099 at either concentration augmented 10 or 100 μM nanoATV-induced inhibition of RT activity by an order of magnitude (Figure 6A, Supplemental Figure 4C). Furthermore, URM-099 (1ng/ml) and nanoATV (10 or 100 μM) inhibited RT activity to its limit of assay detection. Treatment

with native ATV and URM-099 did not affect RT activity levels (Figure 6B, Supplemental Figure 4B).

URM-099 affects nanoATV antiretroviral activities in endosomal compartments

To determine the effect of URM-099 on subcellular trafficking of nanoATV and virus assembly, we posited that decreased Rab7 and -11 expressions might also reflect a decreased number of progeny virions in endosomal compartments. Thus, we measured RT activity in the early, late and recycling endosomes. We isolated Rab compartments from HIV-1 infected cells treated with nanoATV and URM-099, using specific Rab antibody-coated magnetic beads and measured HIV-1 RT activity in each of these compartments (Figure 6C). At 14-days after viral infection, 100 μ M nanoATV alone significantly reduced RT activity in all Rab-labeled endosomal compartments, by 86, 92 and 89% for Rab5, 7- and 11-labeled endosomes, respectively ($p < 0.01$, Figure 6D). Combination of 10 ng/ml URM-099 and 100 μ M nanoATV further decreased RT activity by 38% in Rab5-, 65% in Rab7- and 69% in Rab11-labeled compartments compared to nanoATV alone (Figure 6D).

URM-099 enhances nanoATV retention in Rab7 and -11 endosomes

We reasoned based on deregulation of Rab endosomal proteins by URM-099 and nanoATV and its relationship to antiretroviral responses that the result was linked to retention of the antiretroviral drug at or adjacent to sites of the viral replication cycle. To this end the role of URM-099 in potentiation of nanoATV antiviral activity was measured by assessment of nanoATV uptake and retention in Rab-labeled endosomes. MDM were treated with 100 μ M nanoATV and 10ng/ml URM-099; and endosomal compartments were immuno-isolated. URM-099 had no effect on nanoATV uptake into either whole cells or subcellular compartments (Figure 7A, Supplemental Figure 5). However, 10ng/ml URM-099 significantly enhanced cellular retention of nanoATV from 35.9 to 52.3 μ g ATV/ 10^6 cells at 3 days ($p < 0.05$; Supplemental Figure 5), and increased nanoATV retention in Rab5, -7, and -11 endosomal compartments compared to MDM treated with nanoATV alone ($p < 0.05$; Figure 7B). A simulated flow of nanoparticles and mathematical analyses is presented in Figure 7C and Supplemental Figure 6, which demonstrates the enhanced retention of nanoATV in Rab7 and -11 compartments.

URM-099 enhances nanoATV at sites of virion assembly

We next evaluated the ability of URM-099 to enhance nanoATV accumulation in Rab-labeled endosomal compartments. The co-localization of fluorescently labeled nanoATV with endosomes labeled by fluorescently tagged Rab antibodies were determined in human MDM. URM-099 increased the level of nanoATV in Rab7 and -11 endosomes (Figure 7D-G). Ten ng/ml URM-099 increased nanoATV levels in both Rab7 and -11 endosomes (Figure 7D-G). ATV concentrations persisted to 6 days. As Rab7 and -11 endosomes contain HIV-1 virions, we determined whether HIV-1p24 and nanoATV were co-localized in these organelles (Supplemental Figure 7A-B). Confocal microscopy demonstrated that Rab7- or 11-labeled endosomes (expressed as a coefficient of overlap in a Z-stack of XY images) contained HIV-1p24 and nanoATV. When treated with nanoATV alone, these coefficients of overlap were 0.41 and 0.48, respectively (Supplemental Figure 7C-D). Importantly, they were significantly increased to 0.55 and 0.66 ($p < 0.05$), when URM-099

was co-administered with nanoATV. To explore the relationship by which URM-099 could affect such viral and endosomal drug trafficking we are currently studying, how Rab proteins were regulated in HIV-1 infected and nanoATV-treated macrophages.

Discussion

URM-099 boosts the antiretroviral activities of long-acting nanoART. As progeny virion trafficking occurs largely within these endosomal compartments, the nanoparticle-cell interactions of URM-099 led to improved antiretroviral outcomes. The findings buttress an URM-099-ART marriage by a surprising ability of the drugs to increase ART retention in virus-containing subcellular compartments. This occurred in lymph node viral reservoir compartments. The extension of the half-life of ART by URM-099 provides novel therapeutic opportunities for HIV-1 prevention and buttresses what is now known for nanoART (Figure 8).

The convergence of the drug-drug actions revolves around the therapeutic potential of long-acting nanoART. This is based on the nanoparticles' abilities to maintain effective drug concentration in cellular and tissue depots and thus improve drug pharmacokinetics. Indeed, poorly water-soluble crystalline nanoformulations affect drug stability. Drug particles can also remain within sites of injection in subcutaneous tissue or muscle^{6, 15}. Utilization of peripheral blood mononuclear cells as drug carriers thus presents a novel treatment scheme^{46, 47}. Cell based drug delivery can now be harnessed to improve disease outcomes while overcoming physiologic barriers such as improved drug entry into viral reservoirs^{48, 49}. Such therapeutic enhancements may be further improved by modification of the coating surface of nanoparticles⁵⁰. Targeting ligands, such as FA, mannose, hyaluronic acid or HIV-1gp120, are being developed to facilitate uptake and retention of nanoART^{15, 51}.

The endocytic pathway constitutes the uptake to cells, the out-going route being the biosynthetic pathway⁵². Besides, the endosome is responsible for mediating the uptake of nutrients, the propagation of signaling and regulation of receptors⁵³. The endosomal system also plays an indispensable role in retroviral assembly. The envelope glycoprotein, known as Env, is one of the vital components of a retrovirus, which traffics through the endocytic pathway⁵⁴. Env expressed in infected macrophages is located in intracellular membranes of the endocytic pathway or in trans-Golgi network⁵⁵ HIV-1 assembly in macrophages may occur, in part, from the limiting membrane of a late endosomal compartment linked to in multi-vesicular bodies²⁵. Viruses might be able to hide in these late endosomes, sequestered away from the immune system. What's more, late endosomes and lysosomes are part of the major histocompatibility complex class II compartment, a lysosome-related organelle with properties similar to secretory lysosomes⁵⁶.

Viral particle accumulation can occur inside late endosomes⁵⁷. During native drug administration, such intracellular virus-containing compartments are resistant to antiretroviral drug penetration and retention since less endolysosomal proteins are related to native drug treatment⁵⁸. The modification of the endosomal trafficking route by drug-loaded nanoparticles could significantly improve antiretroviral drug efficacy as our data

demonstrate that HIV-1 can hijack Rab7 and -11 endosomes for virus maturation; this could be circumvented through URM-099. Indeed, URM-099's dual effects on Rab protein regulation and nanoparticle trafficking could lead to improvements in drug action by improving ART delivery to subcellular compartments by several divergent means. *First*, URM-099 can affect redistribution of nanoparticles in the late and recycling endosomes. *Second*, URM-099 cannot, by itself, inhibit HIV-1 replication. *Third*, deactivation of macrophages through suppression of the MAP kinase signaling pathway can restrict transcription of pro-inflammatory cytokine-induced immune responses^{59, 60}. *Fourth*, virus-immune control of Rab protein expression and function is operative⁶¹. Modulation of macrophage activation can affect Rab protein expression and regulate intracellular endocytosis. *Fifth*, progeny virions can be assembled in identical or adjacent compartments affected by immune responses. *Sixth*, this is the first combinatorial formulation known to date to reach the lymph nodes of infected animals and reduce, by more than 90%, the numbers of infectious viral particles. Thus, nanoART and URM-099 would perform synergistic functions by affecting intrinsic macrophage activation. Both would result in reduction of Rab protein expression. Perhaps more importantly, the pharmacologic and pharmacodynamics characteristics of URM-099 bode well for inclusion in the next generation of nanoformulated antiretroviral therapy to combat persistent HIV-1 infection. While targeting viral monocyte-macrophage viral reservoirs is one component that supports the abilities of this cell carriage system to reduce residual HIV-1, nanoparticles encased in cells can affect drug transfer to CD4+ T lymphocytes and improve antiretroviral activities.

Supplementary Material

Refer to Web version on PubMed Central for supplementary material.

Acknowledgments

We thank Aditya Bade, Pavan Puligujja, Edward Makarov, Marnee Roundtree, and Weizhe Li for technical assistance. We thank the UNMC confocal facility for confocal imaging and the Mass Spectrometry and Proteomics Core Facility for proteomics acquisition and analyses.

Funding: This work was supported by the University of Nebraska Foundation which includes individual donations from Dr. Carol Swarts and Frances and Louie Blumkin, the UNMC Vice Chancellor's office and National Institutes of Health grants P01 MH64570, RO1 MH104147 and P30 AI078498 (to H.A.G.) and P01 DA028555, RO1 NS36126, P01 NS31492, 2R01 NS034239, P01 NS43985, P30 MH062261 and R01 AG043540 (to H.E.G.). The funders have had no role in study design.

References

1. Andrews CD, Spreen WR, Mohri H, Moss L, Ford S, Gettie A, et al. Long-acting integrase inhibitor protects macaques from intrarectal simian/human immunodeficiency virus. *Science*. 2014; 343:1151–4. [PubMed: 24594934]
2. Boffito M, Jackson A, Owen A, Becker S. New approaches to antiretroviral drug delivery: challenges and opportunities associated with the use of long-acting injectable agents. *Drugs*. 2014; 74:7–13. [PubMed: 24327298]
3. Mathes T, Antoine SL, Pieper D, Eikermann M. Adherence enhancing interventions for oral anticancer agents: a systematic review. *Cancer Treat Rev*. 2014; 40:102–8. [PubMed: 23910455]
4. Le Moing V, Chene G, Carrieri MP, Alioum A, Brun-Vezinet F, Piroth L, et al. Predictors of virological rebound in HIV-1-infected patients initiating a protease inhibitor-containing regimen. *AIDS*. 2002; 16:21–9. [PubMed: 11741159]

5. Taha H, Morgan J, Das A, Das S. Parenteral Patent Drug S/GSK1265744 has the Potential to be an Effective Agent in Pre-Exposure Prophylaxis Against HIV Infection. *Recent Pat Antiinfect Drug Discov.* 2014
6. Dash PK, Gendelman HE, Roy U, Balkundi S, Alnouti Y, Mosley RL, et al. Long-acting nanoformulated antiretroviral therapy elicits potent antiretroviral and neuroprotective responses in HIV-1-infected humanized mice. *AIDS.* 2012; 26:2135–44. [PubMed: 22824628]
7. Spreen WR, Margolis DA, Pottage JC Jr. Long-acting injectable antiretrovirals for HIV treatment and prevention. *Curr Opin HIV AIDS.* 2013; 8:565–71. [PubMed: 24100877]
8. Guo D, Zhang G, Wysocki TA, Wysocki BJ, Gelbard HA, Liu XM, et al. Endosomal Trafficking of Nanoformulated Antiretroviral Therapy Facilitates Drug Particle Carriage and HIV Clearance. *J Virol.* 2014; 88:9504–13. [PubMed: 24920821]
9. Kadiu I, Nowacek A, McMillan J, Gendelman HE. Macrophage endocytic trafficking of antiretroviral nanoparticles. *Nanomedicine (Lond).* 2011; 6:975–94. [PubMed: 21417829]
10. Tan J, Sattentau QJ. The HIV-1-containing macrophage compartment: a perfect cellular niche? *Trends Microbiol.* 2013; 21:405–12. [PubMed: 23735804]
11. Robillard KR, Chan GN, Zhang G, la Porte C, Cameron W, Bendayan R. Role of P-glycoprotein in the distribution of the HIV protease inhibitor atazanavir in the brain and male genital tract. *Antimicrob Agents Chemother.* 2014; 58:1713–22. [PubMed: 24379203]
12. Dufek MB, Bridges AS, Thakker DR. Intestinal first-pass metabolism by cytochrome p450 and not p-glycoprotein is the major barrier to amprenavir absorption. *Drug Metab Dispos.* 2013; 41:1695–702. [PubMed: 23821186]
13. Marker DF, Tremblay ME, Puccini JM, Barbieri J, Gantz Marker MA, Loweth CJ, et al. The new small-molecule mixed-lineage kinase 3 inhibitor URM-099 is neuroprotective and anti-inflammatory in models of human immunodeficiency virus-associated neurocognitive disorders. *J Neurosci.* 2013; 33:9998–10010. [PubMed: 23761895]
14. Goodfellow VS, Loweth CJ, Ravula SB, Wiemann T, Nguyen T, Xu Y, et al. Discovery, synthesis, and characterization of an orally bioavailable, brain penetrant inhibitor of mixed lineage kinase 3. *J Med Chem.* 2013; 56:8032–48. [PubMed: 24044867]
15. Puligujja P, McMillan J, Kendrick L, Li T, Balkundi S, Smith N, et al. Macrophage folate receptor-targeted antiretroviral therapy facilitates drug entry, retention, antiretroviral activities and biodistribution for reduction of human immunodeficiency virus infections. *Nanomedicine.* 2013; 9:1263–73. [PubMed: 23680933]
16. Puligujja P, Balkundi SS, Kendrick LM, Baldrige HM, Hilaire JR, Bade AN, et al. Pharmacodynamics of long-acting folic acid-receptor targeted ritonavir-boosted atazanavir nanoformulations. *Biomaterials.* 2015; 41:141–50. [PubMed: 25522973]
17. Huang J, Gautam N, Bathena SP, Roy U, McMillan J, Gendelman HE, et al. UPLC-MS/MS quantification of nanoformulated ritonavir, indinavir, atazanavir, and efavirenz in mouse serum and tissues. *J Chromatogr B Analyt Technol Biomed Life Sci.* 2011; 879:2332–8.
18. Gendelman HE, Orenstein JM, Martin MA, Ferrua C, Mitra R, Phipps T, et al. Efficient isolation and propagation of human immunodeficiency virus on recombinant colony-stimulating factor 1-treated monocytes. *J Exp Med.* 1988; 167:1428–41. [PubMed: 3258626]
19. Wisniewski JR, Zougman A, Nagaraj N, Mann M. Universal sample preparation method for proteome analysis. *Nat Methods.* 2009; 6:359–62. [PubMed: 19377485]
20. Huang da W, Sherman BT, Lempicki RA. Bioinformatics enrichment tools: paths toward the comprehensive functional analysis of large gene lists. *Nucleic Acids Res.* 2009; 37:1–13. [PubMed: 19033363]
21. Kanehisa M. The KEGG database. *Novartis Found Symp.* 2002; 247:91–101. discussion 101-3, 119-28, 244-52. [PubMed: 12539951]
22. Kanehisa M, Goto S. KEGG: kyoto encyclopedia of genes and genomes. *Nucleic Acids Res.* 2000; 28:27–30. [PubMed: 10592173]
23. Duan M, Yao H, Hu G, Chen X, Lund AK, Buch S. HIV Tat induces expression of ICAM-1 in HUVECs: implications for miR-221/-222 in HIV-associated cardiomyopathy. *PLoS One.* 2013; 8:e60170. [PubMed: 23555914]

24. Liszewski MK, Yu JJ, O'Doherty U. Detecting HIV-1 integration by repetitive-sampling Alu-gag PCR. *Methods*. 2009; 47:254–60. [PubMed: 19195495]
25. Kumar R, Vandegraaff N, Mundy L, Burrell CJ, Li P. Evaluation of PCR-based methods for the quantitation of integrated HIV-1 DNA. *J Virol Methods*. 2002; 105:233–46. [PubMed: 12270656]
26. Gorantla S, Makarov E, Finke-Dwyer J, Castaneda A, Holguin A, Gebhart CL, et al. Links between progressive HIV-1 infection of humanized mice and viral neuropathogenesis. *Am J Pathol*. 2010; 177:2938–49. [PubMed: 21088215]
27. Nowacek A, Kadiu I, McMillan J, Gendelman HE. Immunoisolation of nanoparticles containing endocytic vesicles for drug quantitation. *Methods Mol Biol*. 2013; 991:41–6. [PubMed: 23546657]
28. Paiardini M, Muller-Trutwin M. HIV-associated chronic immune activation. *Immunol Rev*. 2013; 254:78–101. [PubMed: 23772616]
29. Boswell KL, Paris R, Boritz E, Ambrozak D, Yamamoto T, Darko S, et al. Loss of circulating CD4 T cells with B cell helper function during chronic HIV infection. *PLoS Pathog*. 2014; 10:e1003853. [PubMed: 24497824]
30. Fletcher CV, Staskus K, Wietgreffe SW, Rothenberger M, Reilly C, Chipman JG, et al. Persistent HIV-1 replication is associated with lower retroviral drug concentrations in lymphatic tissues. *Proc Natl Acad Sci U S A*. 2014; 111:2307–12. [PubMed: 24469825]
31. Herbein G, Varin A. The macrophage in HIV-1 infection: from activation to deactivation? *Retrovirology*. 2010; 7:33. [PubMed: 20380696]
32. Levy JA. The importance of the innate immune system in controlling HIV infection and disease. *Trends Immunol*. 2001; 22:312–6. [PubMed: 11377290]
33. Hunt PW, Brenchley J, Sinclair E, McCune JM, Roland M, Page-Shafer K, et al. Relationship between T cell activation and CD4+ T cell count in HIV-seropositive individuals with undetectable plasma HIV RNA levels in the absence of therapy. *J Infect Dis*. 2008; 197:126–33. [PubMed: 18171295]
34. Polesskaya O, Wong C, Lebron L, Chamberlain JM, Gelbard HA, Goodfellow V, et al. MLK3 regulates fMLP-stimulated neutrophil motility. *Mol Immunol*. 2014; 58:214–22. [PubMed: 24389043]
35. Yao M, Liu X, Li D, Chen T, Cai Z, Cao X. Late endosome/lysosome-localized Rab7b suppresses TLR9-initiated proinflammatory cytokine and type I IFN production in macrophages. *J Immunol*. 2009; 183:1751–8. [PubMed: 19587007]
36. Wang Y, Chen T, Han C, He D, Liu H, An H, et al. Lysosome-associated small Rab GTPase Rab7b negatively regulates TLR4 signaling in macrophages by promoting lysosomal degradation of TLR4. *Blood*. 2007; 110:962–71. [PubMed: 17395780]
37. Ciborowski P, Enose Y, Mack A, Fladseth M, Gendelman HE. Diminished matrix metalloproteinase 9 secretion in human immunodeficiency virus-infected mononuclear phagocytes: modulation of innate immunity and implications for neurological disease. *J Neuroimmunol*. 2004; 157:11–6. [PubMed: 15579275]
38. Enose Y, Destache CJ, Mack AL, Anderson JR, Ullrich F, Ciborowski PS, et al. Proteomic fingerprints distinguish microglia, bone marrow, and spleen macrophage populations. *Glia*. 2005; 51:161–72. [PubMed: 15795904]
39. Ciborowski P, Kadiu I, Rozek W, Smith L, Bernhardt K, Fladseth M, et al. Investigating the human immunodeficiency virus type 1-infected monocyte-derived macrophage secretome. *Virology*. 2007; 363:198–209. [PubMed: 17320137]
40. Mellors JW, Griffith BP, Ortiz MA, Landry ML, Ryan JL. Tumor necrosis factor- α /cachectin enhances human immunodeficiency virus type 1 replication in primary macrophages. *J Infect Dis*. 1991; 163:78–82. [PubMed: 1984479]
41. Kraft-Terry SD, Engebretsen IL, Bastola DK, Fox HS, Ciborowski P, Gendelman HE. Pulsed stable isotope labeling of amino acids in cell culture uncovers the dynamic interactions between HIV-1 and the monocyte-derived macrophage. *J Proteome Res*. 2011; 10:2852–62. [PubMed: 21500866]
42. Herbein G, Gras G, Khan KA, Abbas W. Macrophage signaling in HIV-1 infection. *Retrovirology*. 2010; 7:34. [PubMed: 20380698]

43. Caillet M, Janvier K, Pelchen-Matthews A, Delcroix-Genete D, Camus G, Marsh M, et al. Rab7A is required for efficient production of infectious HIV-1. *PLoS Pathog.* 2011; 7:e1002347. [PubMed: 22072966]
44. Pelchen-Matthews A, Kramer B, Marsh M. Infectious HIV-1 assembles in late endosomes in primary macrophages. *J Cell Biol.* 2003; 162:443–55. [PubMed: 12885763]
45. Arainga M, Guo D, Wiederin J, Ciborowski P, McMillan J, Gendelman HE. Opposing regulation of endolysosomal pathways by long-acting formulated antiretroviral therapy and HIV-1 in human macrophages. *Retrovirology.* 2015; 12:5. [PubMed: 25608975]
46. Batrakova EV, Gendelman HE, Kabanov AV. Cell-mediated drug delivery. *Expert Opin Drug Deliv.* 2011; 8:415–33. [PubMed: 21348773]
47. Dou H, Grotepas CB, McMillan JM, Destache CJ, Chaubal M, Werling J, et al. Macrophage delivery of nanoformulated antiretroviral drug to the brain in a murine model of neuroAIDS. *J Immunol.* 2009; 183:661–9. [PubMed: 19535632]
48. Alexaki A, Liu Y, Wigdahl B. Cellular reservoirs of HIV-1 and their role in viral persistence. *Curr HIV Res.* 2008; 6:388–400. [PubMed: 18855649]
49. Chun TW, Fauci AS. HIV reservoirs: pathogenesis and obstacles to viral eradication and cure. *AIDS.* 2012; 26:1261–8. [PubMed: 22472858]
50. Jain NK, Mishra V, Mehra NK. Targeted drug delivery to macrophages. *Expert Opin Drug Deliv.* 2013; 10:353–67. [PubMed: 23289618]
51. Edagwa BJ, Zhou T, McMillan JM, Liu XM, Gendelman HE. Nanomedicine for the Viral Reservoir Drug Delivery and the Fight Against HIV Infection. *Curr Med Chem.* 2014
52. Gruenberg J, van der Goot FG. Mechanisms of pathogen entry through the endosomal compartments. *Nat Rev Mol Cell Biol.* 2006; 7:495–504. [PubMed: 16773132]
53. Miaczynska M, Pelkmans L, Zerial M. Not just a sink: endosomes in control of signal transduction. *Curr Opin Cell Biol.* 2004; 16:400–6. [PubMed: 15261672]
54. Pelchen-Matthews A, Raposo G, Marsh M. Endosomes, exosomes and Trojan viruses. *Trends Microbiol.* 2004; 12:310–6. [PubMed: 15223058]
55. Blot G, Janvier K, Le Panse S, Benarous R, Berlioz-Torrent C. Targeting of the human immunodeficiency virus type 1 envelope to the trans-Golgi network through binding to TIP47 is required for env incorporation into virions and infectivity. *J Virol.* 2003; 77:6931–45. [PubMed: 12768012]
56. Strack B, Calistri A, Craig S, Popova E, Gottlinger HG. AIP1/ALIX is a binding partner for HIV-1 p6 and EIAV p9 functioning in virus budding. *Cell.* 2003; 114:689–99. [PubMed: 14505569]
57. Finzi A, Brunet A, Xiao Y, Thibodeau J, Cohen EA. Major histocompatibility complex class II molecules promote human immunodeficiency virus type 1 assembly and budding to late endosomal/multivesicular body compartments. *J Virol.* 2006; 80:9789–97. [PubMed: 16973583]
58. Chu H, Wang JJ, Qi M, Yoon JJ, Wen X, Chen X, et al. The intracellular virus-containing compartments in primary human macrophages are largely inaccessible to antibodies and small molecules. *PLoS One.* 2012; 7:e35297. [PubMed: 22567100]
59. Kumar S, Boehm J, Lee JC. p38 MAP kinases: key signalling molecules as therapeutic targets for inflammatory diseases. *Nat Rev Drug Discov.* 2003; 2:717–26. [PubMed: 12951578]
60. Kaminska B. MAPK signalling pathways as molecular targets for anti-inflammatory therapy--from molecular mechanisms to therapeutic benefits. *Biochim Biophys Acta.* 2005; 1754:253–62. [PubMed: 16198162]
61. Pei G, Bronietzki M, Gutierrez MG. Immune regulation of Rab proteins expression and intracellular transport. *J Leukoc Biol.* 2012; 92:41–50. [PubMed: 22496357]

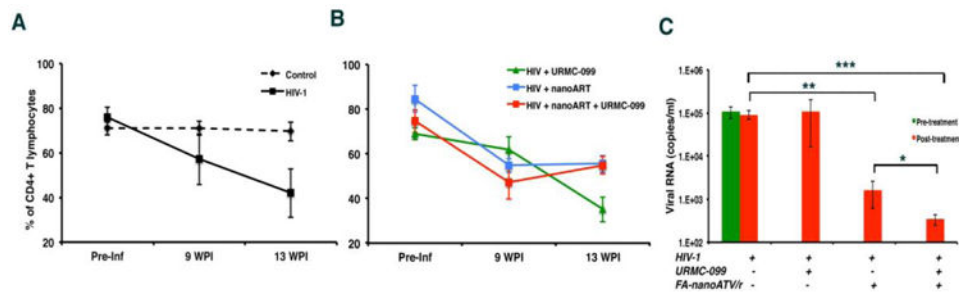


Figure 1. URM-099 potentiates FA-nanoATV/r antiretroviral activities in humanized NSG mice

Humanized NSG mice infected with HIV-1_{ADA} for 10 weeks were administered weekly intramuscular injections of 100 mg/kg FA-nanoATV/r with or without daily IP injections of 10 mg/kg URM-099. All nanoparticles used were coated with FA to facilitate macrophage depot formation. After three weeks, antiviral activity was determined. (A) Human CD4⁺ T cells in peripheral blood during infection in untreated (n=5) and HIV-1 infected (n=5) mice. (B) CD4⁺ T cells in mice treated with FA-nanoATV/r with (n=7)/without URM-099 (n=5) or URM-099 only (n=5) are presented before and after treatment. Preserved CD4⁺ T cell counts in nanoART alone and dual treatment groups were found. The study was repeated 2 times. (C) Plasma viral load measures are illustrated as average \pm SEM. *, **, *** p<0.05.

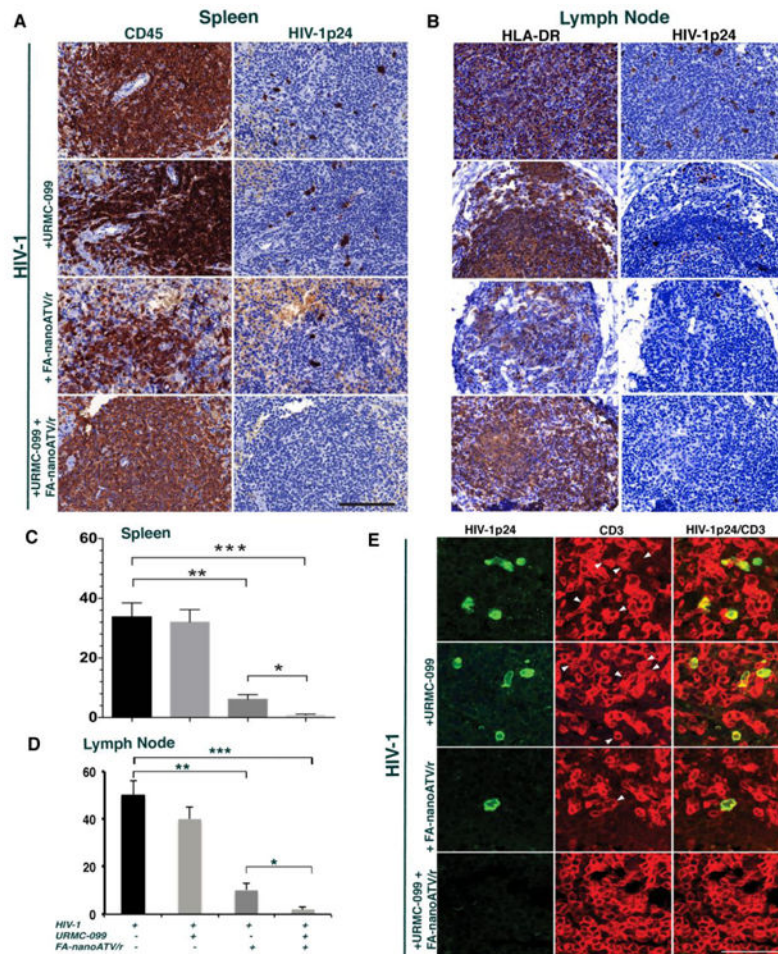


Figure 2. Histopathological evaluation of spleen and lymph nodes from humanized mice (A) Rare HIV-1p24+ cells are seen with FA-nanoATV/r. These were eliminated by the addition of URMC-099. Representative images of human CD45+ and HIV-1p24+ staining (brown) are shown, 40× magnification. Scale bar -100 μm. (C) Lymph nodes showed rare HIV-1p24+ cells in FA-nanoATV/r treated mice, which were eliminated in with URMC-099 co-treatment. (B) Number of HIV-1p24+ cells/1000 human CD45+ cells in spleen and (D) total number of HIV-1p24+ cells in the lymph nodes are shown from five to seven animals/group (average ± SEM). *, **, *** p < 0.05. (E) Immunofluorescence double staining for human CD3+ (red) and HIV-1p24+ (green) cells in spleen demonstrated that HIV-1p24 infected cells are T lymphocytes. URMC-099 co-treatment with FA-nanoATV7r reduces residual lymphocyte infection in spleen. White arrows point to T lymphocytes that are HIV-1p24+. 100× magnification. Scale bar equals 50μm.

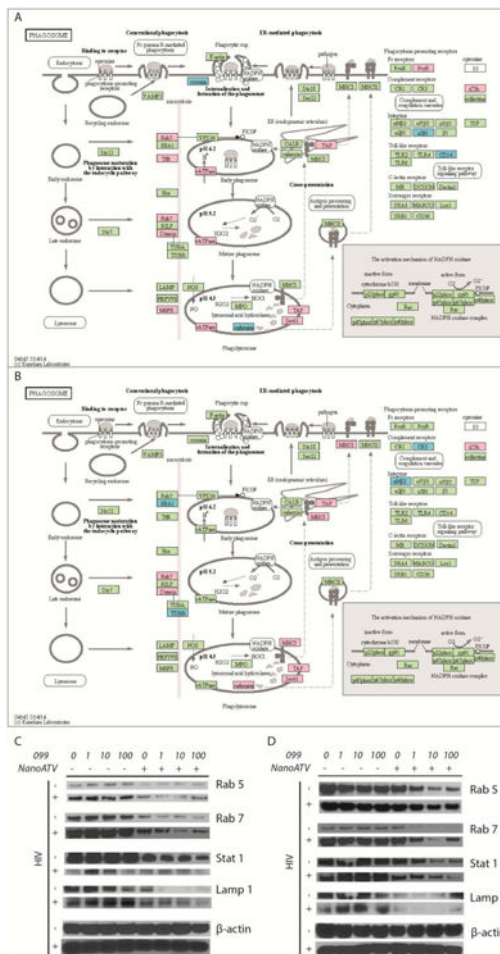


Figure 3. Schematic representation of the MDM phagosome network
 MDM phagosome network identified in (A) HIV-1-infected and (B) HIV-1-infected with URMC-099 and nanoATV treated cells. Proteins identified were compared against uninfected MDM cultures ($p < 0.05$). The acquired profiles were analyzed through the bioinformatics tools DAVID and KEGG Pathway. Statistical significance was determined using a p -value < 0.05 . Proteins in red and blue, display up- and down- regulation, respectively. Proteins in green belong to the phagosome network and not deregulated by ATV treatment. URMC-099 deregulates phagosomal protein expressions in human MDM. The proteomics data were based on experiments conducted from 4 donor MDMs. MDM were treated with $100\mu\text{M}$ nanoATV for 16 hours with 0, 1, 10 or 100 ng/mL URMC-099. HIV-1_{ADA} infection was performed at (C) day 0 or (D) day 5 after drug treatment. Cell lysates were collected on day 7 following infection. Expression of Rab5, Rab7, STAT1, and LAMP1 were determined by Western blot in URMC-099/nanoATV treated MDM. Results are from a representative experiment. Western blots were performed in duplicates from 2 donor MDMs.

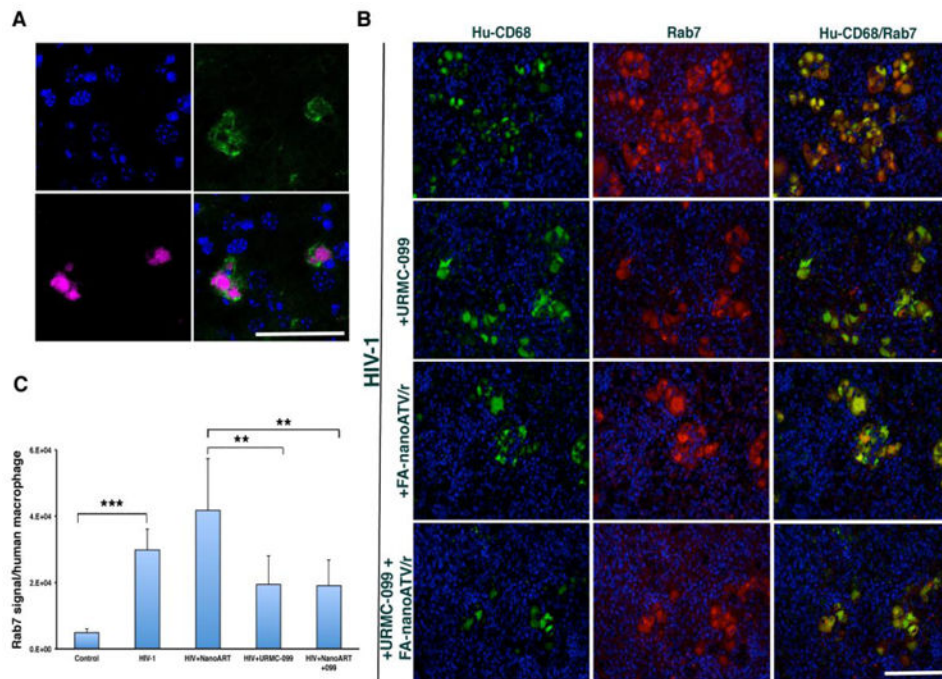


Figure 4. Nanoparticle uptake and characterization of Rab7 expression in human macrophages with HIV-1 infection

(A) Liver showed the presence of CF633 labeled nanoATV (red) in mouse macrophages (F4/80-green), demonstrating clear uptake and co-localization of nanoATV in tissue resident macrophages. Results were confirmed using 5 mice. (B) Immunofluorescence double staining of human macrophages (CD68-green) and human Rab7 (red) in spleens of humanized mice showed an increase in the expression of co-localized Rab7 in HIV-1 infected or FA-nanoATV/r (n=5) treated groups compared to uninfected controls, infected mice treated with URMC-099 alone (n=5) or double treatment (n=7) and (C) significant increase in expression in HIV-1 infected group as compared to controls. *, **, *** $p < 0.05$. Scale bar equals 100 μm (Figure 4A), 50 μm (Figure 4B).

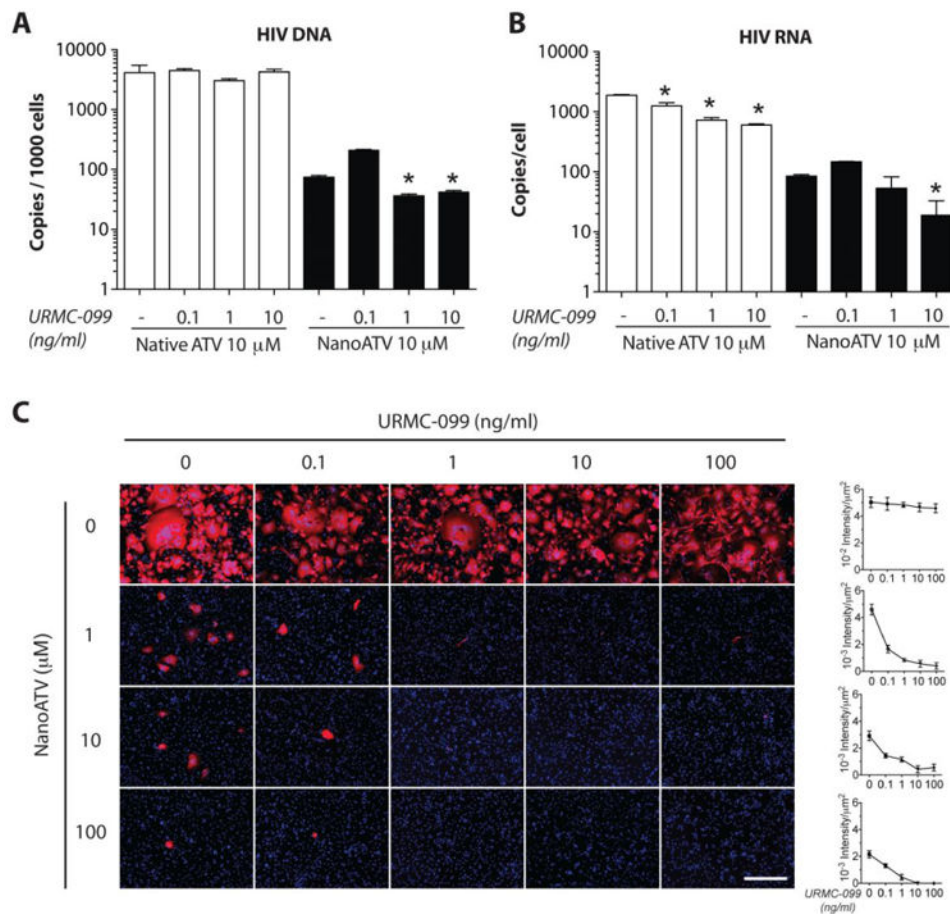


Figure 5. URM-099 potentiates nanoATV antiretroviral activities in HIV-1 infected MDM
 URM-099 and native ATV or nanoATV treated human MDM were infected with HIV-1_{ADA} and cultured for 14 days. (A) HIV-1 LTR DNA was measured by Alu-gag PCR amplification (n = 4). (B) HIV-1 RNA was measured by HIV-1 gag amplification (n = 4); * p<0.05 compared to ATV treatment without URM-099. (C) Immunocytochemical staining of HIV-1p24 expression (red). Nuclei are stained with DAPI (blue). Immunofluorescence was quantified and is expressed as mean \pm SEM. 100 \times Magnification. Scale bar -100 μ m.

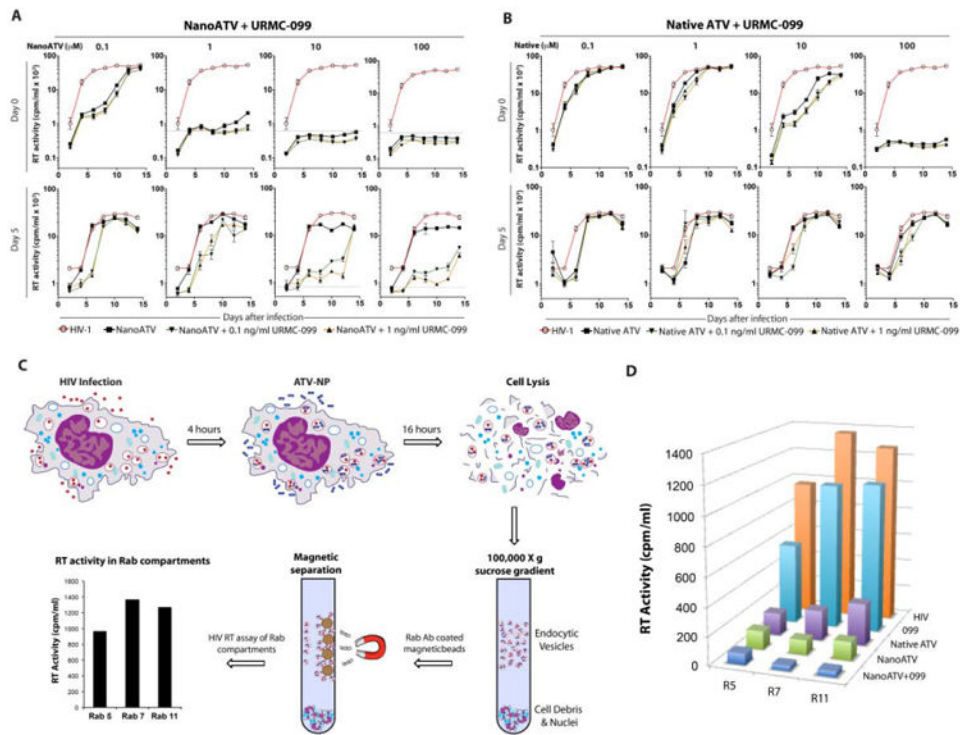


Figure 6. URMC-099 prolongs antiretroviral activities of nanoATV in HIV-1-infected human MDM

MDM were treated with URMC-099 (0.1 or 1 ng/ml) and native ATV or nanoATV (100 μ M) for 8 hours, and infected with HIV-1_{ADA} at day 0 or day 5 after drug treatment. HIV-1 RT activity was measured in culture supernatants 14 days after infection. RT activity in MDM treated with (A) nanoATV and URMC-099 or (B) native ATV and URMC-099 are shown. Gray line = limit of detection for assay. Data are expressed as average \pm SEM (n=4). (C) Endosomal compartments isolated from URMC-099 (10 ng/ml), native ATV or nanoATV (100 μ M) treated MDM 14 days after HIV-1 infection were evaluated for RT activity. (D) HIV-1 RT activity was determined in Rab (R) -5, -7 and -11 positive compartments. Average activities of n=5 replicates are shown.

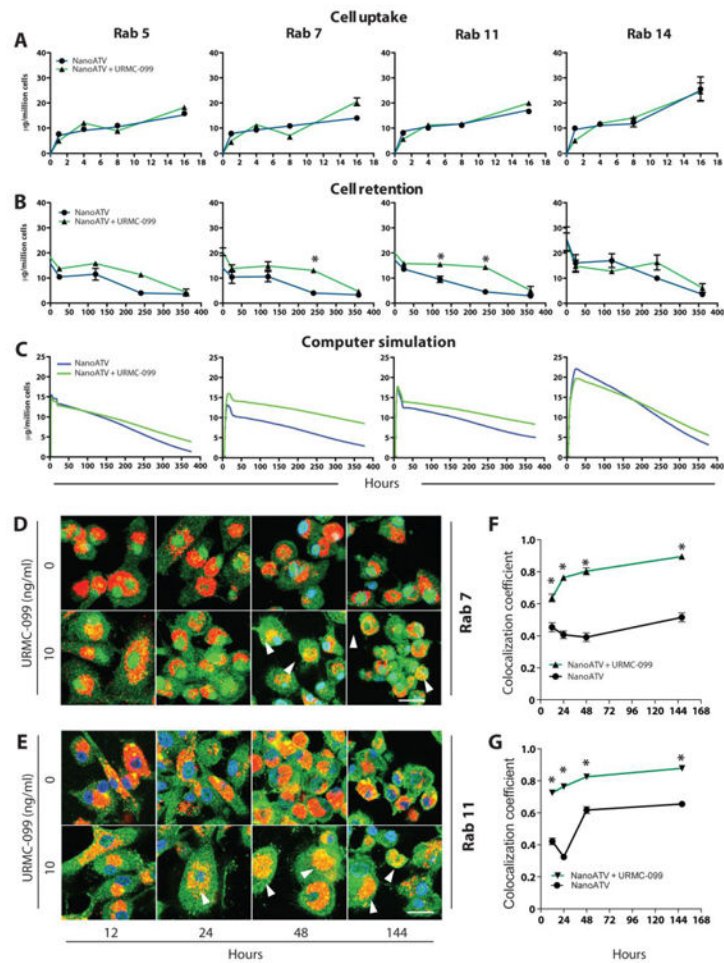


Figure 7. URM-099 facilitates retention of nanoATV in endosomal compartments
 Human MDM were treated with 100 μ M nanoATV with or without 10 ng/ml URM-099 for 16 hours then maintained for an additional 15 days. Subcellular compartments were isolated by immunoaffinity chromatography using antibody coated magnetic beads. **(A)** MDM nanoATV drug levels into individual endosomal compartments over 16 hours were measured. **(B)** Retention of nanoATV over 15 days (360 hours) in endosomes after the 16-hour loading (average \pm SEM, n=5). All cell retention and uptake studies are repeated 3 times. **(C)** Mathematical simulation of nanoATV retention in individual endosomal compartments over the same time frame. **(D)** URM-099 potentiates nanoATV accumulation in Rab7 endosomal compartments. **(E)** URM-099 increases nanoATV accumulation in Rab11 endosomal compartments. **(D and E)** Arrowheads point to dual labeled Rab and nanoparticles. CF568-labeled nanoATV shows as red, while AlexaFluor 488-labeled endosomal compartment shows as green. DAPI (blue) indicates cell nuclei, 1260 \times magnification. Percent overlap of nanoATV with **(F)** Rab7 and **(G)** -11 was quantitated (average \pm SEM, n=30, unpaired 2-tailed t-test); * p<0.05 compared to respective time point. Scale bar =20 μ m.

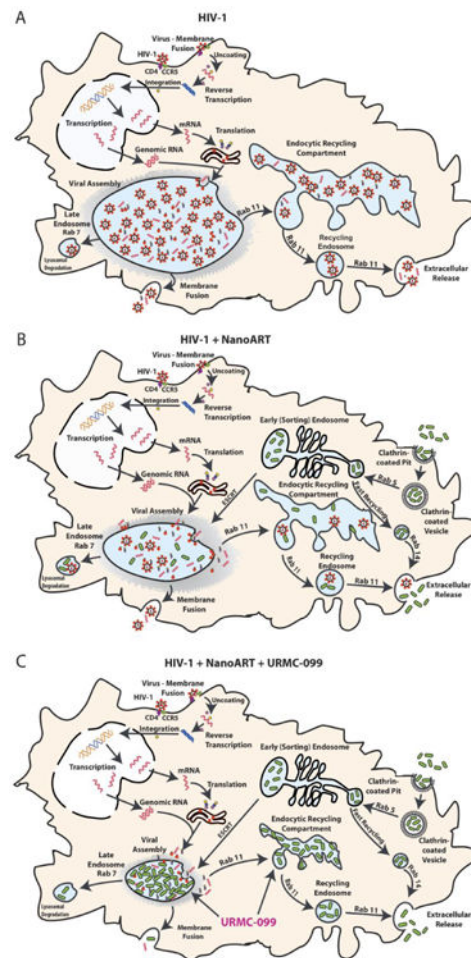
















Figure 8. Schematic diagrams reveal URM-099 affects nanoART endosomal trafficking and HIV-1 progeny virion production

(A) HIV-1 budding, assembly and maturation in macrophage Rab7 and Rab11 endosomal compartments. (B) NanoART targets endosomal compartment for storage and inhibits viral maturation at the site of viral assembly. (C) URM-099 boosts nanoART antiviral activity through increased nanoART accumulation in macrophage Rab7 and Rab11 endosomal compartments.

Table 1
Endolysosomal proteins in HIV-1 or nanoATV+099 treated MDM

Protein	HIV-1		HIV+nanoATV+099	
	Z test	Regulation	Z test	Regulation
Rab5	4.22		--	
TAP	2.39		2.11	
TFR	3.91		--	




HIV-1		HIV+nanoATV+099	
Protein	Ztest	Regulation	Z test
vATPase	4.48		--
Stx13	--		--
EEA1	--		-3.27
VPS34	--		--
CALR	--		--
Calnexin	--		--
			Regulation




	HIV-1		HIV+nanoATV+099	
Protein	Z test	Regulation	Z test	Regulation
Rab7	2.12		2.89	
vATPase	4.48		--	
Dynein	4.49		5.27	
TUBB	--		-3.38	

Late endosomes

HIV-1		HIV+nanoATV+099	
Protein	Z test	Regulation	Z test
TUBA	--		
RILP	--		
Six7	--		
LAMP	--		
vATPase	4.48		
TAP	2.39		

Lysosomes

HIV-1		HIV+nanoATV+099	
Protein	Ztest	Regulation	Z test
M6PR	2.00		--
Cathepsin	-2.52		3.17
			

 Downregulated
 Unchanged
 Upregulated